ELSEVIER

Biophysical Chemistry 113 (2005) 67–81

Biophysical Chemistry

www.elsevier.com/locate/bpc

A fractal analysis of pathogen detection by biosensors

Bret A. Morris, Ajit Sadana*

Chemical Engineering Department, University of Mississippi, Post Office Box 1848, University, MS 38677-1848, USA

Received 6 April 2004; received in revised form 15 July 2004; accepted 19 July 2004
Available online 27 September 2004

Abstract

A fractal analysis is presented for the detection of pathogens such as *Franscisela tularensis*, *Yersinia pestis* (the bacterium that causes plague), *Bacillus anthracis*, Venezuelan equine encephalitis (VEE) virus, Vavcinia virus, and *Escherichia coli* using a cellular analysis and notification of antigens risks and yields (CANARY) biosensor [T.H. Rider, M.S. Petrovic, F.E. Nargi, J.D Harper, E.D. Schwoebel, R.H. Mathews, D.J. Blanchard, L.T Bortolin, A.M. Young, J. Chen, M.A. Hollis, A cell-based sensor for rapid identification of pathogens, Science 301 (2003, 11 July) 213–215, T.H. Rider, M.S. Petrovic, F.E. Nargi, J.D. Harper, E.D. Schwoebel, R.H. Mathews, D.J. Blanchard, L.T. Bortolin, A.M. Young, J. Chen, M.A. Hollis, A cell-based sensor for rapid identification of pathogens, Science 301 (2003, 11 July) 213–215. Science Online, www.sciencemag.org/cgi/content/full/031/5630/213/DC1]. In general, the binding and dissociation rate coefficients may be adequately described by either a single- or a dual-fractal analysis. An attempt is made to relate the binding rate coefficient to the degree of heterogeneity (fractal dimension value) present on the biosensor surface. Binding and dissociation rate coefficient values obtained are presented.

Due to the dilute nature of the analyte(s) present, in some cases, a triple-fractal analysis is required to adequately describe the binding kinetics. It should be noted, and this is not entirely unexpected, that there is a lot of variation in the original experimental data when dilute concentrations of the analyte were analyzed by the CANARY biosensor [T.H. Rider, M.S. Petrovic, F.E. Nargi, J.D Harper, E.D. Schwoebel, R.H. Mathews, D.J. Blanchard, L.T Bortolin, A.M. Young, J. Chen, M.A. Hollis, A cell-based sensor for rapid identification of pathogens, Science 301 (2003, 11 July) 213–215, Science Online, www.sciencemag.org/cgi/content/full/031/5630/213/DC1]. The data analyzed in this manuscript appears smoother since only discrete points at different time intervals were analyzed. The kinetics aspects along with the affinity values presented are of interest and should along with the rate coefficients presented for the binding and the dissociation phase be of significant interest in help designing better biosensors for an application area that is bound to gain increasing importance in the future.

Keywords: Pathogen detection; Biosensors; Analyte receptor kinetics

1. Introduction

The development of biosensors was until recently propelled mainly by medical applications. Recent events on a global level have thrusted the applications of biosensors to the detection of chemical and biological agents of mass destruction. Note that in both medical and in national security applications, one needs to detect viruses and pathogens at rather low levels and in dilute concentrations. The principles of application and development in both areas exhibit similarities, with the major difference being that in most medical applications, pathogens are not immediately life-threatening, in contrast to security applications when there may be merely minutes to hours [1] (a) to take corrective action to remove or to neutralize the pathogen and (b) to remove the endangered civilian and military personnel from the affected areas. The identification of exotic and lethal diseases most frequently associated with biological weapons programs is a slow, uncertain, and fragmented process.

There was and continues to be increasing pressure to enhance biosensor performance characteristics such as

* Corresponding author. Tel.: +1 662 915 5349/7023; fax: +1 662 915 5349.

0301-4622/$ - see front matter © 2004 Elsevier B.V. All rights reserved.
doi:10.1016/j.bpc.2004.07.041

stability, sensitivity, response time, robustness, selectivity, and regeneration. The biosensor system for destructive biological agents requires not only the detection of a harmful biological agent but also its identification. A three-step process may be necessary that includes a detection step, an identification step, and finally a communication step for alarm and/or control systems Furthermore, this agent is often present in a very dilute solution, and there is an urgent need to minimize false positives. Biological and chemical agents can be present in different types of situations such as military applications, forensics, law enforcement, and medical diagnostics [2]. Each of these situations will have common themes as well as characteristics that are unique to their particular application. In a broad sense, one can present some underlying principles which may have general applicability with the caveat that these may have to be modified to one's particular application. It is imperative to develop fast, accurate, and reliable detection systems for pathogens. The ultimate aim is to provide a continuous monitoring system.

Fitch et al. [2] have recently outlined the technology challenges one may expect in the civilian sector when responding to chemical and biological attacks. As expected, there is a plethora of activity in the governmental, industrial, and academic areas to promote the development of biosensors not only in the chemical and biological detection area for military applications but also, for example, making edible food safe. Some of the techniques used for the detection of biological agents include optical biosensors [3], structure–function based biosensors [17], and time-of-flight mass spectrometry and laser-induced fluorescence [4]. As expected, nanotechnology has played [5] and will continue to play a major role in the detection of pathogenic agents. Most of these detection systems should be portable. The Defense Advanced Research Projects Agency [6] in its Sensor Integration and Modeling for Biological Agent Detection (SIMBAD) program is developing tools and methodologies that will result in a significant increase in its understanding of biological warfare detection technologies. The program encompasses a complete system that includes monitoring capabilities and a reporting aspect that indicates the presence or absence of a threat.

As an example, the detection of pathogens may be underscored by the very recent mad-cow disease event that occurred in the north-western part of the United States, and the implications it has (or may have) on the economy of certain areas, and the fall-out of such an event. The present detection technique involves immunodiagnostic techniques, and its expense per test is partly to blame. Sveshnikov [7] has indicated the need for rapid and sensitive immunoassays for pathogen detection. Cheaper and more reliable techniques, such as involving biosensors with more frequent testing, would help minimize such events that tend to create instability locally, as well as perhaps globally to some extent.

The kinetics of binding and dissociation of analytes present in solution or in the environment to (complementary) receptors immobilized on a biosensor surface is an important step that provides information not only on the biomolecular interaction taking place on the biosensor surface but also assists significantly in improving biosensor performance parameters such as stability, selectivity, response time, sensitivity, etc.

A number of biowarfare agents, such as botulinum toxin, ricin, and Staphylococcus enterotoxins, are proteins [8]. The binding kinetics of cholera toxin (CT) in solution to fluorophore-labeled ganglioside GM1 immobilized on a biomimetic membrane surface [9] has been analyzed using fractal methods [18]. Rider et al. [10,11] have recently presented data for the rapid detection of pathogens such as *Franscisella tularensis*, *Yersinia pestis* (the bacterium that causes plague), *Bacillus anthracis*, Venezuelan equine encephalitis (VEE) virus, and *Escherichia coli*. Note that the first four have defense or military applications, whereas the last one helps keep edible food safe. They used a B lymphocytes cell based sensor named cellular analysis and notification of antigens risks and yields (CANARY). No kinetic analysis for either the binding or the dissociation phase was available. In this manuscript, we reanalyze the data by Rider et al. [10,11] using a fractal analysis to provide kinetic rate coefficients for the binding and the dissociation phase. Affinity values are also provided. The fractal dimension values presented provide an indication of the degree of heterogeneity present on the biosensor surface. In no way are we indicating that the present analysis is in any way better than the original analysis by [10,11]. The present analysis should just be considered as an alternate analysis. A unique feature of the analysis of fractals to the present system is the very dilute nature of the analyte(s) present in the atmosphere. The kinetics provided in the manuscript should complement and enhance the original [10,11] analysis.

2. Theory

Havlin [12] has reviewed and analyzed the diffusion of reactants towards fractal surfaces. The details of the theory and the equations involved for the binding and the dissociation phases for analyte–receptor binding are available [13]. The details are not repeated here; except that just the equations are given to permit an easier reading. These equations have been applied to other biosensor systems [13,14]. Here we will attempt to apply these equations to the rapid detection of pathogens using a B cell-based biosensor [10,11]. We recognize that these systems are very dilute. To accommodate this very dilute nature of these systems, a triple-fractal analysis may be used if necessary. For most applications, a single- or a dual-fractal analysis is often adequate to describe the binding and the dissociation kinetics. Peculiarities in the values of the

binding and the dissociation rate coefficients, as well as in the values of the fractal dimensions with regard to the dilute analyte systems being analyzed will be carefully noted, if applicable.

2.1. Single-fractal analysis

2.1.1. Binding rate coefficient

Havlin [12] indicates that the diffusion of a particle (analyte [Ag]) from a homogeneous solution to a solid surface (e.g., receptor [Ab]-coated surface) on which it reacts to form a product (analyte–receptor complex; (Ab · Ag)) is given by:

$$(\mathrm{Ab}\cdot\mathrm{Ag}) \approx \begin{cases} t^{(3-\mathrm{D_{f,bind}})/2} = t^{p} & t<t_c \\ t^{1/2} & t>t_c \end{cases} \quad (1a)$$

where $D_{f,bind}$ or D_f (used later on in the manuscript) is the fractal dimension of the surface during the binding step, and t_c is the cross-over value. The binding rate coefficient, k, is the proportionality coefficient of Eq. (1a). Havlin [12] indicates that the cross-over value may be determined by $r_c^2 \sim t_c$. Above the characteristic length, r_c, the self-similarity of the surface is lost and the surface may be considered homogeneous. Above time, t_c the surface may be considered homogeneous, since the self-similarity property disappears, and 'regular' diffusion is now present. For a homogeneous surface where D_f is equal to 2, and when only diffusional limitations are present, p=1/2 as it should be. Another way of looking at the p=1/2 case (where $D_{f,bind}$ is equal to two) is that the analyte in solution views the fractal object, in our case, the receptor-coated biosensor surface, from a 'large distance.' Following along the lines of the Havlin [12] analysis, in essence, in the association (or binding) process, the diffusion of the analyte from the solution to the receptor surface creates a depletion layer of width $(Đt)^{1/2}$, where Đ is the diffusion constant. This gives rise to the fractal power law, (Analyte.Receptor)$\sim t^{(3-\mathrm{D_{f,bind}})/2}$. For the present analysis, t_c is arbitrarily chosen and we assume that the value of the t_c is not reached. One may consider the approach as an intermediate 'heuristic' approach that may be used in the future to develop an autonomous (and not time-dependent) model for diffusion-controlled kinetics.

It is instructive to examine the units of the binding rate coefficient, k. Assume that that the concentration of the antibody.antigen (Ab · Ag) complex on the biosensor surface has the units, ng/cm^2. Then, Eq. (1a) may be written as:

$$(\mathrm{Ab}\cdot\mathrm{Ag})\left(\mathrm{ng/cm^2}\right) = kt^{(3-\mathrm{D_f})/2}$$

Time, t has the units (s); thus, the units of the binding rate coefficient, k, are (ng/cm^2) (s)$^{(3-\mathrm{D_f})/2}$. Note that the binding rate coefficient, k, has a temporal value which is a characteristic of fractallike kinetics.

2.1.2. Dissociation rate coefficient

The diffusion of the dissociated particle (receptor [Ab] or analyte [Ag]) from the solid surface (e.g., analyte [Ag]–receptor [Ab]) complex-coated surface) into solution may be given, as a first approximation by:

$$(\mathrm{Ab}\cdot\mathrm{Ag}) \approx -t^{(3-\mathrm{D_{f,diss}})/2} \qquad t>t_{\mathrm{diss}} \quad (1b)$$

Here, $D_{f,diss}$ is the fractal dimension of the surface for the dissociation step. Time t_{diss} is the start of the dissociation step. This corresponds to the highest concentration of the analyte–receptor complex on the surface. Henceforth, its concentration only decreases. The dissociation kinetics may be analyzed in a manner 'similar' to the binding kinetics.

Similarly, as in the binding step, the dissociation rate coefficient, k_d is the proportionality coefficient of Eq. (1b). In the dissociation phase, and as indicated above, the concentration of (Ab · Ag) is continuously decreasing. The negative sign indicates this decrease. By definition, a rate coefficient, binding or dissociation is positive.

2.2. Dual-fractal analysis

Sometimes, the binding curve exhibits complexities and two parameters (k, D_f) are not sufficient to adequately describe the binding kinetics. This is further corroborated by low values of r^2 factor (goodness-of-fit). In that case, one resorts to a dual-fractal analysis (four parameters: k_1, k_2, D_{f1}, and D_{f2}) to adequately describe the binding kinetics. The single-fractal analysis presented above is thus extended to include two fractal dimensions. At present, the time (t=t_1) at which the 'first' fractal dimension 'changes' to the 'second' fractal dimension is arbitrary and empirical. For the most part, it is dictated by the data analyzed and experience gained by handling a single-fractal analysis. A smoother curve is obtained in the 'transition' region, if care is taken to select the correct number of points for the two regions. In this case, the product (antibody–antigen; or analyte–receptor complex, Ab · Ag or analyte.receptor) is given by:

$$(\mathrm{Ab}\cdot\mathrm{Ag}) \approx \begin{cases} t^{(3-\mathrm{D_{f1,bind}})/2} = t^{p1} & t<t_1 \\ t^{(3-\mathrm{D_{f2,bind}})/2} = t^{p2} & t_1<t<t_2 \\ t^{1/2} & t>t_c \end{cases} \quad (1c)$$

In this case, the binding rate coefficient, k_1 is the proportionality coefficient for the Eq. (1c) that applies for time, t<t_1. Similarly, the binding rate coefficient, k_2 is the proportionality coefficient for the Eq. (1c) that applies for time, t_1<t<t_2. A similar units analysis may be made for the binding rate coefficients, k_1 and k_2 that apply during the first and second phase of binding. The units for k_1 and k_2 are (ng/cm^2)(s)$t^{(3-\mathrm{D_{f1}})/2}$ and (ng/cm^2)(s)$t^{(3-\mathrm{D_{f2}})/2}$, respectively. In some cases, as mentioned above, a triple-fractal analysis with six parameters (k_1, k_2, k_3, D_{f1}, D_{f2}, and D_{f3}) may be required to adequately model the binding kinetics. This is when the binding curve exhibits convolutions and complex-

ities in its shape due to perhaps to the very dilute nature of the analyte (in some of the cases to be presented) or for some other reasons. Also, in some cases, a dual-fractal analysis may be required to describe the dissociation kinetics.

3. Results

The fractal analysis will be applied to the rapid identification of pathogens using a B-cell based biosensor [10,11].

Alternate expressions for fitting the data are available that include saturation, first-order reaction, and no diffusion limitations, but these expressions are apparently deficient in describing the heterogeneity that inherently exists on the surface. One might justifiably argue that appropriate modeling may be achieved by using a Langmuirian or other approach. The Langmuirian approach may be used to model the data presented if one assumes the presence of discrete classes of sites (for example, double exponential analysis as compared with a single-fractal analysis). [19] indicate that the fractal approach has been applied to surface science, for example, adsorption and reaction processes. These authors emphasize that the fractal approach provides a convenient means to represent the different structures and morphology at the reaction surface. These authors also emphasize using the fractal approach to develop optimal structures and as a predictive approach. Another advantage of the fractal technique is that the analyte–receptor association (as well as the dissociation reaction) is a complex reaction, and the fractal analysis via the fractal dimension and the rate coefficient provide a useful lumped parameter(s) analysis of the diffusion-limited reaction occurring on a heterogeneous surface.

In a classical situation, to demonstrate fractality, one should make a log–log plot, and one should definitely have a large amount of data. It may be useful to compare the fit to some other forms such as exponential or one involving saturation, etc. At present, we do not present any independent proof or physical evidence of fractals in the examples presented. It is a convenient means (since it is a lumped parameter) to make the degree of heterogeneity that exists on the surface more quantitative. Thus, there is some arbitrariness in the fractal model to be presented. The fractal approach provides additional information about interactions that may not be obtained by conventional analysis of biosensor data.

There is no nonselective adsorption of the analyte. The present system (pathogens) being analyzed is typically very dilute. Nonselective adsorption would skew the results obtained very significantly. In these types of systems, it is imperative to minimize this nonselective adsorption. We also do recognize that in some cases, this nonselective adsorption may not be a significant component of the adsorbed material and that this rate of association, which is of a temporal nature, would depend on surface availability. If we were to accommodate the nonselective adsorption into the model, there would be an increase in the heterogeneity on the surface since, by its very nature, nonspecific adsorption is more homogeneous than specific adsorption. This would lead to higher fractal dimension values since the fractal dimension is a direct measure of the degree of heterogeneity that exists on the surface.

Rider et al. [10,11] have used a B-cell based biosensor to rapidly analyze pathogens. They emphasize that there is a need to rapidly identify bioterrorism agents compared to present immunoassays [15]. They have used the CANARY (cellular analysis and notification of antigen risks and yields) biosensor to rapidly identify pathogens such as *Y. pestis*, *F. tularensis*, *B. Anthracis*, and the Venezuelan equine encephalitis (VEE) virus. Fig. 1A shows the binding of 500 cfu *Y. Pestis* to pathogen-specific B cells immobilized on a biosensor surface. A dual-fractal analysis is required to adequately describe the binding kinetics. The dissociation kinetics is adequately described by a single-fractal analysis. The values of (a) the binding rate coefficient, k, for a single-fractal analysis, (b) the binding rate coefficients, k_1 and k_2, for a dual-fractal analysis, and (c) the dissociation rate coefficient, k_d, for a single-fractal analysis are presented in Table 1A. The values of (a) the fractal dimension, D_f, for binding for a single-fractal analysis, (b) the fractal dimensions, D_{f1} and D_{f2}, for binding for a dual-fractal analysis, and (c) the fractal dimension, D_{fd}, for the dissociation phase for a single-fractal analysis are presented in Table 1B. Due to the 'convex' nature (S-shaped curve) of the binding curve at time, t, close to zero, the fractal dimension value is estimated to be equal to zero. This indicates that the surface acts as a "Cantor' like dust.

Define affinity, K_1 as k_1/k_d and K_2 as k_2/k_d. Then, K_1 is equal to 4.057, and K_2 is equal to 0.545. The affinity value decreases by a factor of 7.44 on going from the first phase (K_1) of the binding curve to the second phase (K_2) of the binding curve.

Fig. 1B shows the binding of 50 cfu *Y. Pestis* to pathogen-specific B cells immobilized on a biosensor surface. Once again, a dual-fractal analysis is required to adequately describe the binding kinetics. The dissociation kinetics is adequately described by a single-fractal analysis. The values of (a) the binding rate coefficient, k, for a single-fractal analysis, (b) the binding rate coefficients, k_1 and k_2, for a dual-fractal analysis, and (c) the dissociation rate coefficient, k_d, for a single-fractal analysis are presented in Table 1A. The values of (a) the fractal dimension, D_f, for binding for a single-fractal analysis, (b) the fractal dimensions, D_{f1} and D_{f2}, for binding for a dual-fractal analysis, and (c) the fractal dimension, D_{fd}, for the dissociation phase are presented in Table 1B. In this case, since the binding curve does not exhibit a S-shaped curve at time, t close to zero, the fractal dimension value, D_{f1} is equal to 1.8414 when the dual-fractal analysis applies. Also, in this case, K_1 is equal to 3.126 and K_2 is equal to 3.035. At this low value of the analyte concentration (50 cfu *Y. Pestis*), there is a very

small decrease (2.91%) in the affinity value as one goes from the first to the second phase of binding.

Fig. 1C shows the binding of 50 cfu *Y. Pestis* and 5×10^5 cfu *F. tularensis* to pathogen-specific B cells immobilized on a biosensor surface. In this case, both the binding as well as the dissociation kinetics are adequately described by a single-fractal analysis. The values of (a) the binding rate coefficient, k, and the dissociation rate coefficient, k_d, for a single-fractal analysis are presented in Table 1A. The values of the fractal dimension, D_f, for binding for a single-fractal

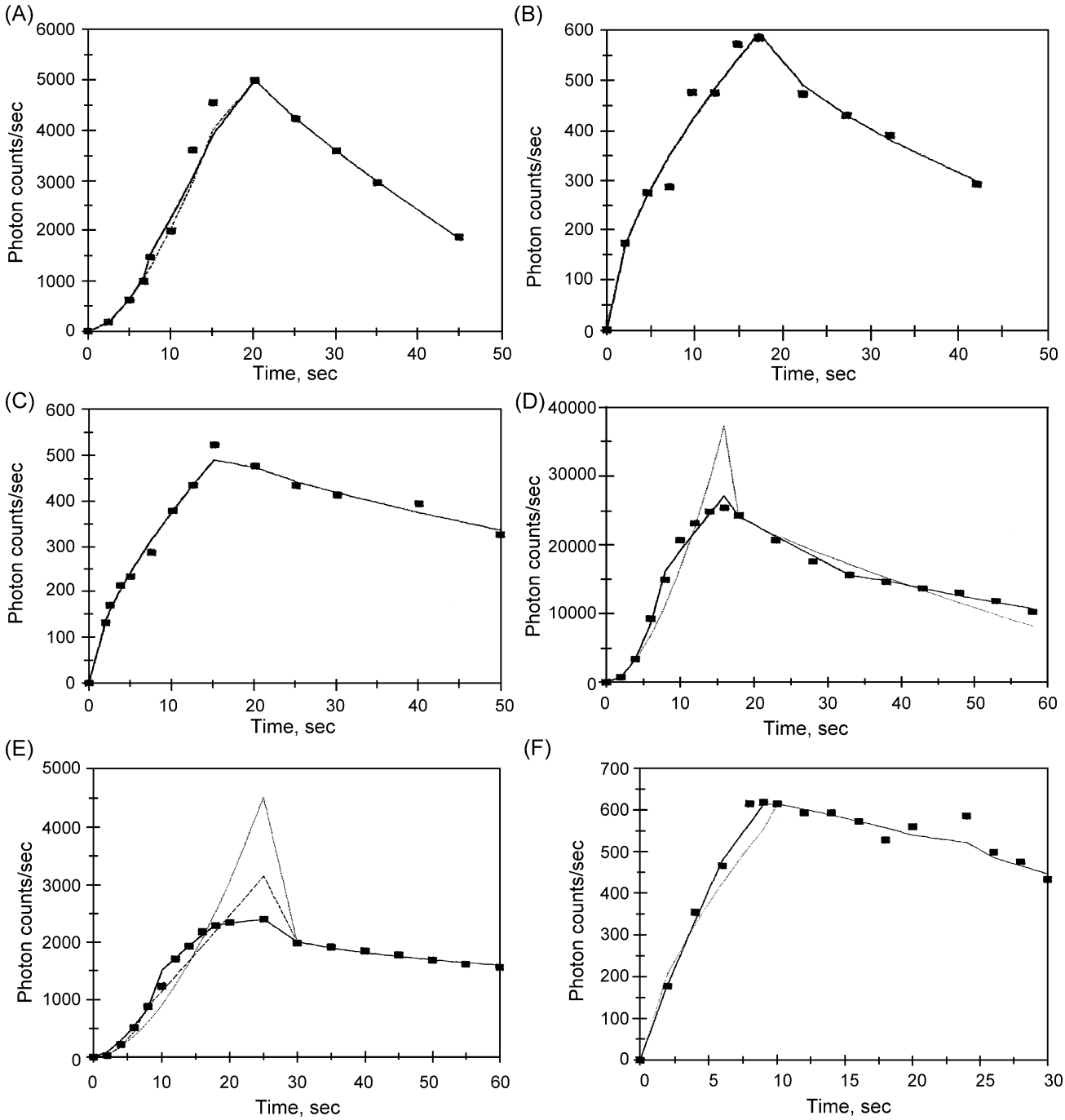

Fig. 1. Binding and dissociation curves for the detection of different pathogens at different concentrations by B lymphocyte-based sensor [10,11]: (A) 500 cfu *Y. pestis*; (B) 50 cfu *Y. pestis*; (C) 50 cfu *Y. pestis*+5×10^5 cfu *F. tularensis*; (D) 5000 pfu Vaccinia virus; (E) 500 pfu Vaccinia virus; (F) 1000 cfu *E. coli* 0157:H7; (G) 500 cfu *E. coli* 0157:H7; (H) 5×10^7 pfu Venezuelan equine encephalitis (VEE TC 83); (I) 5×10^6 pfu Venezuelan equine encephalitis (VEE TC 83); (J) 5×10^6 pfu Venezuelan equine encephalitis (VEE TC 83); and (K) 10,000 cfu *B. anthracis* spores, (L) 1000 cfu *B. anthracis* spores. When only a solid line (—) is used, then a single-fractal analysis applies. When a dashed (- - -) and a solid line (—) is used, then the dashed line represents a single-fractal analysis and the solid line represents a dual-fractal analysis. When a dashed (- - -), a dotted (. . .) and a solid line (—) is used, then the dashed line represents a single-fractal analysis, the dotted line represents a dual-fractal analysis, and the solid line represents a triple-fractal analysis.

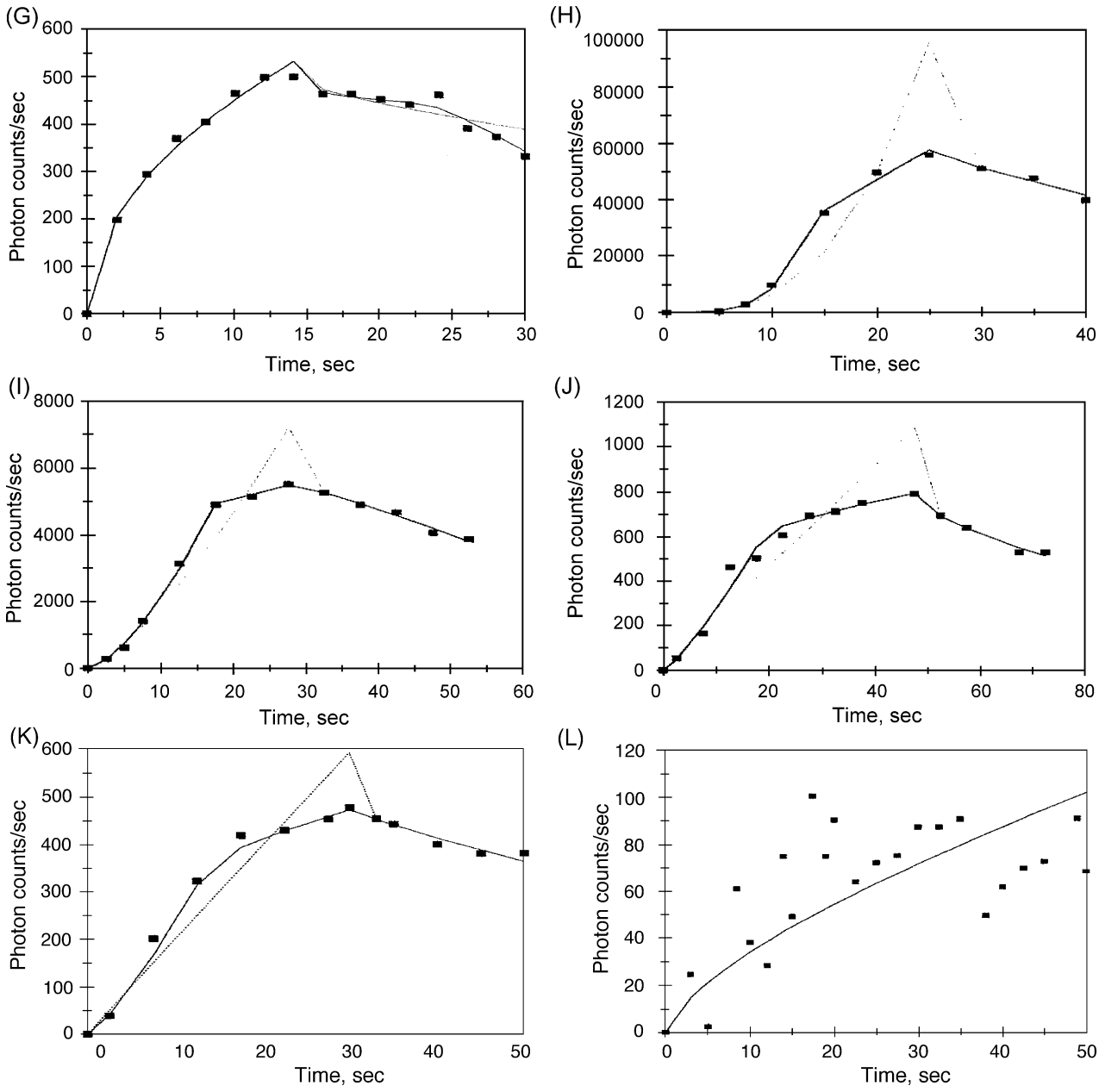

Fig. 1 (*continued*).

analysis and the fractal dimension, D_{fd}, for the dissociation phase for a single-fractal analysis are presented in Table 1B. In this case since the binding curve does not exhibit a S-shaped curve at time, t close to zero, the fractal dimension value, D_f, is equal to 1.7311 for the single-fractal analysis. Since a single-fractal analysis applies to both the binding and the dissociation phases, the affinity, K ($=k/k_d$), value is 5.29.

Fig. 1D shows the binding of 5000 pfu Vaccinia virus to pathogen specific B cells immobilized on a biosensor surface. In this case, a dual-fractal analysis is required to describe the binding as well as the dissociation phases. The values of (a) the binding rate coefficient, k, for a single-fractal analysis, (b) the binding rate coefficients, k_1 and k_2, for a dual-fractal analysis, (c) the dissociation rate coefficient, k_d, for a single-fractal analysis, and (d) the dissociation rate coefficients, k_{d1} and k_{d2}, for a dual-fractal analysis are presented in Table 1A. The values of (a) the fractal dimension, D_f, for binding for a single-fractal analysis, (b) the fractal dimensions, D_{f1} and D_{f2}, for binding for a dual-fractal analysis, (c) the fractal dimension, D_{fd}, for the dissociation phase for a single-fractal analysis, and (d) the fractal dimensions, D_{fd1} and D_{fd2}, for dissociation for a dual-fractal analysis are presented in Table 1B. In this case, since a dual-fractal analysis is required to adequately describe both the binding as well as the dissociation phases,

Table 1A
Binding and dissociation rate coefficients for different pathogens on a B lymphocyte-based sensor [10,11]

Pathogen concentration	k	k_1	k_2	k_3	k_d	k_{d1}	k_{d2}
(a)							
500 cfu *Yersinia pestis*	43.99±7.72	36.21±3.95	97.28±18.4	na	178.49±2.33	na	na
50 cfu *Yersinia pestis*	110.64±12.93	113.02±16.68	109.73±16.38	na	36.15±3.49	na	na
50 cfu *Yersinia pestis*+5×10^5 cfu *Francisella tularensis*	88.27±5.76	na	na	na	16.68±2.11	na	na
(b)							
Vaccinia Virus, 5000 pfu	304.31±100.40	167.98±14.67	3344.32±287.5	na	838.55±161.9	651.11±99.26	2340.55±66.87
Vaccinia Virus, 500 pfu	16.14±7.99	31.17±1.99	268.6±5.57	1529.6±2.19	200.68±11.62	na	na
(c)							
Escherichia coli 0157: H7 1000 cfu	133.65±22.71	98.38±4.68	145.22±9.17	na	4.188±1.21	na	na
Escherichia coli 0157: H7 500 cfu	147.44±6.32	na	na	na	15.40±8.08	25.94±3.78	0.7785±0.376
(d)							
Venezuelan equine encephalitis (VEE TC83) virus, 5×10^7 pfu	7.1750±4.36	1.229±0.197	2946.9±216.3	na	890.56±167.6	na	na
Venezuelan equine encephalitis (VEE TC83) virus, 5×10^6 pfu	85.08±20.07	62.94±10.61	2341.91±34.93	na	38.35±3.85	na	na
Venezuelan equine encephalitis (VEE TC83) virus, 5×10^5 pfu	26.46±6.47	15.90±3.90	278.68±3.04	na	33.82±2.61	na	na
B. anthracis spores 10,000 cfu	20.88±6.19	13.66±2.61	149.25±2.41	na	9.878±1.60	na	na
B. anthracis spores 1000 cfu	7.008±5.97	7.008±5.97	34.769±4.589	0.2492±0.036	na	na	na

let us define the affinity, K_1 as k_1/k_{d1} and K_2 as k_2/k_{d2}. Then, using this definition, K_1 is equal to 0.258 and K_2 is equal to 1.423.

Fig. 1E shows the binding of 500 pfu Vaccinia virus to pathogen specific B cells immobilized on a biosensor surface. In this case, due to the complexities exhibited by the binding curve at this lower or dilute Vaccinia virus concentration, a triple-fractal analysis is required to adequately describe the binding kinetics. A single-fractal analysis is, however, sufficient to adequately describe the dissociation phase. The values of (a) the binding rate coefficient, k, for a single-fractal analysis, (b) the binding rate coefficients, k_1, k_2, and k_3, for a triple-fractal analysis, and (c) the dissociation rate coefficient, k_d, for a single-fractal analysis are presented in Table 1A. The values of (a) the fractal dimension, D_f, for binding for a single-fractal analysis, (b) the fractal dimensions, D_{f1}, D_{f2}, and D_{f3}, for binding for a triple-fractal analysis, and (c) the fractal dimension, D_{fd}, for the dissociation phase for a single-fractal analysis are presented in Table 1B. Once again, define affinity, K_1 as k_1/k_d, K_2 as k_2/k_d, and K_3 as k_3/k_d. Then, K_1 is equal to 0.155, K_2 is equal to 1.428, and K_3 is equal to 7.62. As one goes from the first phase to the second phase and then on to the third phase of binding, the affinity value keeps on increasing. It increases by a factor of 9.21 on going from the first phase to the second phase and by a factor of 5.34 on going from the second phase to the third phase.

Fig. 1F shows the binding of 1000 cfu *E. coli* 0157:H7 to pathogen-specific B cells immobilized on a biosensor surface. Once again, a dual-fractal analysis is required to adequately describe the binding kinetics. The dissociation kinetics is adequately described by a single-fractal analysis. The values of (a) the binding rate coefficient, k, for a single-fractal analysis, (b) the binding rate coefficients, k_1 and k_2, for a dual-fractal analysis, and (c) the dissociation rate coefficient, k_d, for a single-fractal analysis are presented in Table 1A. The values of (a) the fractal dimension, D_f, for binding for a single-fractal analysis, (b) the fractal dimensions, D_{f1} and D_{f2}, for binding for a dual-fractal analysis, and (c) the fractal dimension, D_{fd}, for the dissociation phase for a single-fractal analysis are presented in Table 1B. In this case, K_1 is equal to 23.49 and K_2 is equal to 34.68. There is an increase by a factor of 1.48 in the affinity value as one goes from the first to the second phase of binding.

Fig. 1G shows the binding of 500 cfu *E. coli* 0157:H7 to pathogen-specific B cells immobilized on a biosensor surface. A single-fractal analysis is required to adequately describe the binding kinetics. The dissociation kinetics is adequately described by a dual-fractal analysis. The values

Table 1B
Fractal dimensions for binding and dissociation for different pathogens on a B lymphocyte-based sensor [10,11]

Pathogen concentration	D_f	D_{f1}	D_{f2}	D_{f3}	D_{fd}	D_{fd1}	D_{fd2}
(a)							
500 cfu *Yersinia pestis*	0+0.1845	0+0.240	0.2656±0.4624	na	1.2194±0.022	na	na
50 cfu *Yersinia pestis*	1.8084±0.1944	1.8414±0.1944	1.8306±0.2736	na	1.7032±0.1272	na	na
50 cfu *Yersinia pestis*+5×10^5 cfu *Francisella tularensis*	1.7311±0.0639	na	na	na	1.6513±0.1554	na	na
(b)							
Vaccinia Virus, 5000 pfu	0+0.3064	0+0.160	1.4872±0.301	na	1.3790±0.1282	1.0796±0.1492	2.0138±0.1102
Vaccinia Virus, 500 pfu	0+0.3350	0+0.1854	1.5084±0.1359	2.7204±0.0669	2.2654±0.0610	na	na
(c)							
Escherichia coli 0157: H7 1000 cfu	1.7036±0.1846	1.2292±0.0892	1.6870±0.1658	na	0.5650±0.1782	na	na
Escherichia coli 0157: H7 500 cfu	2.0220±0.050	na	na	na	1.6084±0.4534	2.3412±0.2614	0+1.4388
(d)							
Venezuelan equine encephalitis (VEE-TC83) virus, 5×10^7 pfu	0+0.6948	0+0.3702	1.1522±0.3910	na	0.9930±0.439	na	na
Venezuelan equine encephalitis (VEE-TC83) virus, 5×10^6 pfu	0.3214±0.1990	0+0.2648	2.4864±0.0924	na	0.6240±0.1506	na	na
Venezuelan equine encephalitis (VEE-TC83) virus, 5×10^5 pfu	1.0770±0.1900	0.5908±0.2980	2.4578±0.0800	na	1.6910±0.1176	na	na
(e)							
Bacillus anthracis spores 10,000 cfu	1.0344±0.2402	0.5202±0.2374	2.3250±0.1534	na	1.3600±0.1922	na	na
Bacillus anthracis spores 1000 cfu	1.6382±0.3578	1.0882±0.4962	2.494±0.4182	0.0424+1.0896	na	na	na

of (a) the binding rate coefficient, k, for a single-fractal analysis, (b) the dissociation rate coefficient, k_d, for a single-fractal analysis, and (c) the dissociation rate coefficient, k_{d1} and k_{d2}, for a dual-fractal analysis are presented in Table 1A. The values of (a) the fractal dimension, D_f, for binding for a single-fractal analysis, (b) the fractal dimension, D_{fd}, for the dissociation phase for a single-fractal analysis, and (c) the fractal dimensions, D_{fd1} and D_{fd2}, for dissociation for a dual-fractal analysis are presented in Table 1B. In this case, K_1 is equal to 5.68 and K_2 is equal to 189.38. There is an increase by a factor of 33.34 in the affinity value as one goes from the first to the second phase of binding.

Fig. 1H shows the binding of 5×10^7 pfu of the Venezuelan equine encephalitis (VEE TC83) virus to pathogen-specific B cells immobilized on a biosensor surface. A dual-fractal analysis is required to adequately describe the binding kinetics. The dissociation kinetics is adequately described by a single-fractal analysis. The values of (a) the binding rate coefficient, k, for a single-fractal analysis, (b) the binding rate coefficients, k_1 and k_2, for a dual-fractal analysis, and (c) the dissociation rate coefficient, k_d, for a single-fractal analysis are presented in Table 1A. The values of (a) the fractal dimension, D_f, for binding for a single-fractal analysis, (b) the fractal dimensions, D_{f1} and D_{f2}, for binding for a dual-fractal analysis, and (c) the fractal dimension, D_{fd}, for the dissociation phase for a single-fractal analysis are presented in Table 1B. In this case, K_1 is equal to 0.00138 and K_2 is equal to 3.31. There is an increase by a factor of 2398.5 in the affinity value as one goes from the first to the second phase of binding.

Fig. 1I shows the binding of 5×10^6 pfu of the Venezuelan equine encephalitis (VEE TC83) virus to pathogen-specific B cells immobilized on a biosensor surface. A dual-fractal analysis is required to adequately describe the binding kinetics. The dissociation kinetics is adequately described by a single-fractal analysis. The values of (a) the binding rate coefficient, k, for a single-fractal analysis, (b) the binding rate coefficients, k_1 and k_2, for a dual-fractal analysis, and (c) the dissociation rate coefficient, k_d, for a single-fractal analysis are presented in Table 1A. The values of (a) the fractal dimension, D_f, for binding for a single-fractal analysis, (b) the fractal dimensions, D_{f1} and D_{f2}, for binding for a dual-fractal analysis, and (c) the fractal dimension, D_{fd}, for the dissociation phase for a single-fractal analysis are presented in Table 1B. In this case, K_1 is equal to 1.641 and K_2 is equal to 61.85. There is

an increase by a factor of 37.69 in the affinity value as one goes from the first to the second phase of binding.

Fig. 1J shows the binding of 5×10^5 pfu of the Venezuelan equine encephalitis (VEE TC83) virus to pathogen-specific B cells immobilized on a biosensor surface. A dual-fractal analysis is required to adequately describe the binding kinetics. The dissociation kinetics is adequately described by a single-fractal analysis. The values of (a) the binding rate coefficient, k, for a single-fractal analysis, (b) the binding rate coefficients, k_1 and k_2, for a dual-fractal analysis, and (c) the dissociation rate coefficient, k_d, for a single-fractal analysis are presented in Table 1A. The values of (a) the fractal dimension, D_f, for binding for a single-fractal analysis, (b) the fractal dimensions, D_{f1} and D_{f2}, for binding for a dual-fractal analysis, and (c) the fractal dimension, D_{fd}, for the dissociation phase for a single-fractal analysis are presented in Table 1B. In this case, K_1 is equal to 0.47 and K_2 is equal to 8.24. There is an increase by a factor of 17.53 in the affinity value as one goes from the first to the second phase of binding.

Fig. 1K shows the binding of 10,000 cfu of *B. anthracis* spores to pathogen-specific B cells immobilized on a biosensor surface. A dual-fractal analysis is required to adequately describe the binding kinetics. The dissociation kinetics is adequately described by a single-fractal analysis. The values of (a) the binding rate coefficient, k, for a single-fractal analysis, (b) the binding rate coefficients, k_1 and k_2, for a dual-fractal analysis, and (c) the dissociation rate coefficient, k_d, for a single-fractal analysis are presented in Table 1A. The values of (a) the fractal dimension, D_f, for binding for a single-fractal analysis, (b) the fractal dimensions, D_{f1} and D_{f2}, for binding for a dual-fractal analysis, and (c) the fractal dimension, D_{fd}, for the dissociation phase for a single-fractal analysis are presented in Table 1B. In this case, K_1 is equal to 1.383 and K_2 is equal to 15.11. There is an increase by a factor of 10.93 in the affinity value as one goes from the first to the second phase of binding.

Fig. 1L shows the binding of 1000 cfu of *B. anthracis* spores to pathogen-specific B cells immobilized on a biosensor surface. At this low concentration of *B. anthracis* spores only a binding phase is exhibited. However, a triple-fractal analysis is required to adequately describe the binding kinetics. The values of (a) the binding rate coefficient, k, for a single-fractal analysis, and (b) the binding rate coefficients, k_1, k_2, and k_3, for a triple-fractal analysis are presented in Table 1A. The values of (a) the fractal dimension, D_f, for binding for a single-fractal analysis, and (b) the fractal dimensions, D_{f1}, D_{f2}, and D_{f3}, for binding for a triple-fractal analysis are presented in Table 1B. Since no dissociation phase was exhibited here, no affinity values are presented.

Fig. 2A shows that the binding rate coefficient, k_1, increases with an increase in the fractal dimension, D_{f1}. The binding rate coefficient, k_1, is given by:

$$k_1 = (46.59\pm17.51)D_{f1}^{1.842\pm0.306} \quad (2a)$$

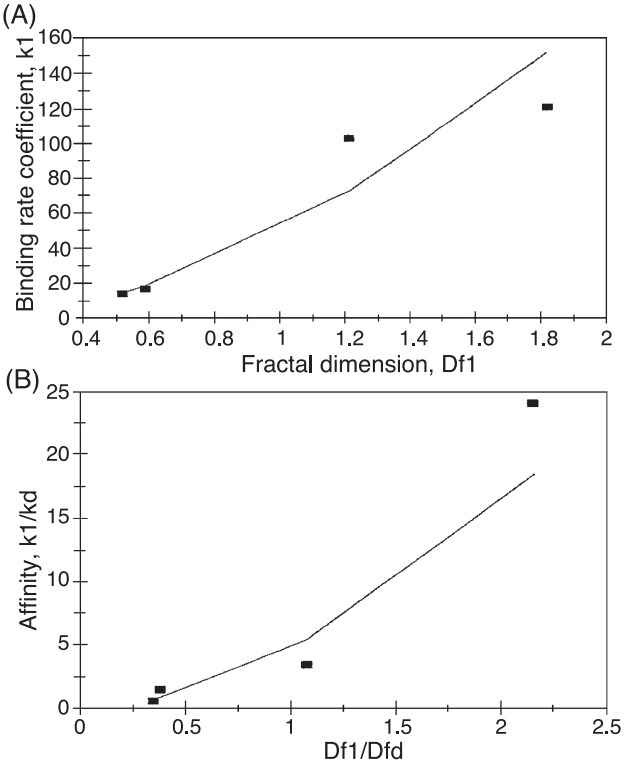

Fig. 2. (A) Increase in the binding rate coefficient, k_1 with an increase in the fractal dimension, D_{f1} (B) Increase in the affinity, $K(=k_1/k_d)$ with an increase in the fractal dimension ratio, D_{f1}/D_{fd}.

The binding rate coefficient, k_1, is quite sensitive to the degree of heterogeneity on the biosensor surface as noted by the 1.842 order of dependence on the fractal dimension, D_{f1}. Only four data points were available. More data points are required to make the curve more reliable.

Fig. 2B shows that the affinity, $K_1(=k_1/k_d)$, increases with an increase in the fractal dimension ratio, D_{f1}/D_{fd}. The affinity binding rate coefficient, K_1, is given by:

$$K_1 = (4.4221\pm3.7486)(D_{f1}/D_{fd})^{1.7975\pm0.404} \quad (2b)$$

The affinity, K_1, is quite sensitive to the degree of heterogeneity on the biosensor surface as noted by the 1.842 order of dependence on the fractal dimension, D_{f1}. Only four data points were available. More data points are required to make the curve more reliable.

Fig. 3A shows the binding of 25 μl of B cells+5 μl pRMC strain at 1.4×10^8 pfu/ml (wt. A12FMDV) to pathogen-specific B cells immobilized on a biosensor surface. A triple-fractal analysis is required to adequately describe the binding kinetics. No dissociation curve is exhibited. The values of (a) the binding rate coefficient, k, for a single-fractal analysis, (b) the binding rate coefficients, k_1, k_2, and k_3, for a triple-fractal analysis are presented in Table 2A. The values of (a) the fractal dimension, D_f, for binding for a single-fractal analysis, and (b) the fractal dimensions, D_{f1}, D_{f2}, and D_{f3}, for binding for a triple-fractal analysis are presented in Table 2B.

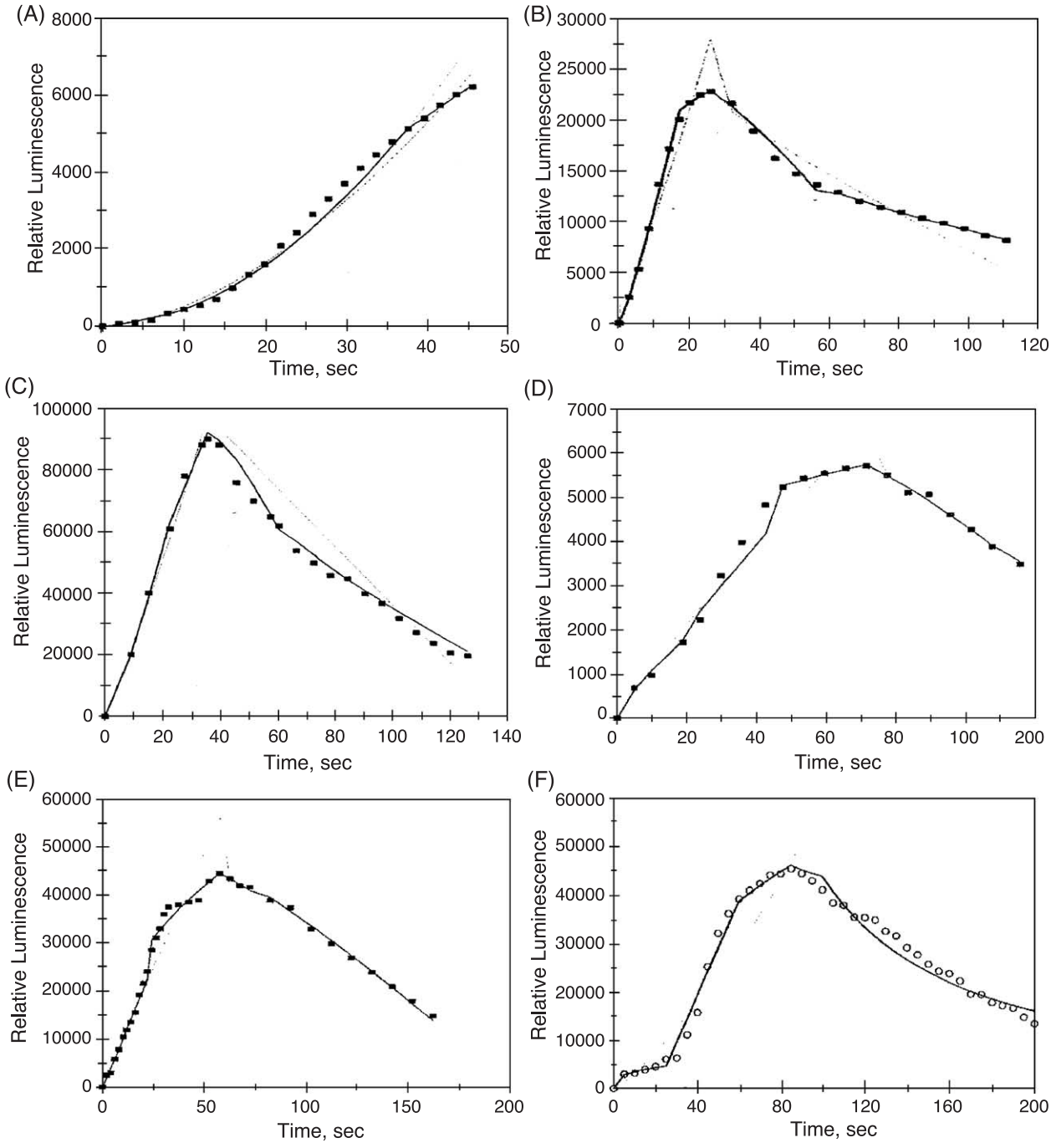

Fig. 3. Binding and dissociation curves for the detection of different pathogens at different concentrations by B lymphocyte-based sensor (Rider et al., [10,11] supplement, 2003): (A) 25 μl of B cells+5 μl pRMC35 strain at 1.4×10^8 pfu/ml (wt. A12 FMDV); (B) 20 μl of B cells+Venezuelan equine encephalitis (VEE) virus strain subtype 1A TC-83; (C) 20 μl of B cells+Venezuelan equine encephalitis (VEE) virus strain subtype 1BPTF-39; (D) 20 μl of B cells+Venezuelan equine encephalitis (VEE) virus strain subtype 1c p676; (E) 20 μl of B cells+Venezuelan equine encephalitis (VEE) virus strain 3880 subtype 1d; and (F) 20 μl of B cells+Venezuelan equine encephalitis (VEE) virus strain subtype 1e (Mena II).

Fig. 3B shows the binding of 20 μl of B cells+VEE virus strain subtype 1A TC83 to pathogen-specific B cells immobilized on a biosensor surface. A dual-fractal analysis is required to adequately describe the binding as well as the dissociation kinetics. The values of (a) the binding rate coefficient, k, for a single-fractal analysis, (b) the binding rate coefficients, k_1 and k_2, for a dual-fractal analysis, (c) the dissociation rate coefficient, k_d, for a single-fractal analysis, and (d) the dissociation rate coefficients, k_{d1} and k_{d2}, for a dual-fractal analysis are presented in Table 2A. The values of (a) the fractal dimension, D_f, for binding for a single-fractal analysis, (b) the fractal dimensions, D_{f1} and D_{f2}, for binding for a dual-fractal analysis, (c) the fractal dimension, D_{fd}, for the dissociation phase for a single-fractal analysis,

Table 2A
Binding and dissociation rate coefficients for different pathogens on a B lymphocytes-based sensor (Rider et al. [10,11], Science Supplement)

Pathogen concentration	k	k_1	k_2	k_3	k_d	k_{d1}	k_{d2}
25 μl of B cells+5 μl pRMC35 strain at 1.4×10^8 pfu/ml (wt. A12 FMDV)	9.738±2.499	19.689±6.136	5.011±0.549	114.60±0.808	na	na	na
20 μl of B cells+Venezuelan equinine encephalitis (VEE) virus strain subtype 1A TC-83	843.72±115.87	653.99±36.21	11,810.9±96.53	na	441.89±107.55	171.67±37.06	2013.48±16.64
20 μl of B cells+Venezuelan equinine encephalitis (VEE) virus strain subtype 1B PTF-39	1834.40±141.98	1293.41±60.12	4825.63±211.30	na	978.17±277.66	400.26±132.03	3814.72±100.17
20 μl of B cells+Venezuelan equinine encephalitis (VEE) virus strain subtype 1c p676	148.69±20.08	206.28±19.23	125.44±16.63	na	24.38±3.44	na	na
20 μl of B cells+Venezuelan equinine encephalitis (VEE) virus strain 3880 subtype 1d	1095.06±176.56	999.35±138.35	7744.63±391.14	na	159±18.3	na	na
20 μl of B cells+Venezuelan equinine encephalitis (VEE) virus strain subtype 1e (Mena II)	178.53±84.54	1799.10±150.1	4.145±0.921	5146.31±97.32	4.82 E+07±0.45 E+07	na	na

Table 2B
Fractal dimensions for the binding and dissociation phase for different pathogens on a B lymphocytes-based sensor (Rider et al. [10,11], Science Supplement)

Pathogen concentration	D_f	D_{f1}	D_{f2}	D_{f3}	D_{fd}	D_{fd1}	D_{fd2}
25 μl of B cells+5 μl pRMC35 strain at 1.4×10^8 pfu/ml (wt. A12 FMDV)	0	0.4598±0.0324	0+0.107	0.9246±0.094	na	na	na
20 μl of B cells+Venezuelan equinine encephalitis (VEE) virus strain subtype 1A TC-83	0.8790±0.126	0.6044±0.073	2.6014±0.092	na	1.3302±0.156	171.67±37.06	2013.48±16.64
20 μl of B cells+Venezuelan equinine encephalitis (VEE) virus strain subtype 1B PTF-39	0.7662±0.128	0.493±0.143	1.3408±0.235	na	1.0196±0.149	0.2904±0.338	1.7058±0.0466
20 μl of B cells+Venezuelan equinine encephalitis (VEE) virus strain subtype 1c p676	1.2316±0.094	21.5498±0.146	1.1402±0.1864	na	0.5946±0.157	na	na
20 μl of B cells+Venezuelan equinine encephalitis (VEE) virus strain 3880 subtype 1d	1.0528±0.076	0.9892±0.110	2.1334±0.1086	na	0.720±0.068	na	na
20 μl of B cells+Venezuelan equinine encephalitis (VEE) virus strain subtype 1e (Mena II)	0.5052±0.243	2.4224±0.154	0+0.4328	2.0162±0.0978	0+0.1568	na	na

and (d) the fractal dimensions, D_{fd1} and D_{fd2}, for dissociation for a dual-fractal analysis are presented in Table 2B. In this case, K_1 ($=k_1/k_{d1}$) is equal to 3.81 and K_2 ($=k_2/k_{d2}$) is equal to 5.87. The affinity value increases by a factor of 1.54 as one goes from the first to the second phase of binding.

Fig. 3C shows the binding of 20 μl of B cells+VEE virus strain subtype 1BPTF-39 to pathogen-specific B cells immobilized on a biosensor surface. A dual-fractal analysis is required to adequately describe the binding as well as the dissociation kinetics. The values of (a) the binding rate coefficient, k, for a single-fractal analysis, (b) the binding rate coefficients, k_1 and k_2, for a dual-fractal analysis, (c) the dissociation rate coefficient, k_d, for a single-fractal analysis, and (d) the dissociation rate coefficients, k_{d1} and k_{d2}, for a dual-fractal analysis are presented in Table 2A. The values of (a) the fractal dimension, D_f, for binding for a single-fractal analysis, (b) the fractal dimensions, D_{f1} and D_{f2}, for binding for a dual-fractal analysis, (c) the fractal dimension, D_{fd}, for the dissociation phase, and (d) the fractal dimensions, D_{fd1} and D_{fd2} for the dissociation phase are presented in Table 2B. In this case, K_1 is equal to 3.23 and K_2 is equal to 1.265. The affinity value decreases by a factor of 2.55 as one goes from the first to the second phase of binding.

Fig. 3D shows the binding of 20 μl of B cells+VEE virus strain subtype 1cp676 to pathogen-specific B cells immobilized on a biosensor surface. A dual-fractal analysis is required to adequately describe the binding kinetics. The dissociation kinetics is adequately described by a single-fractal analysis. The values of (a) the binding rate coefficient, k, for a single-fractal analysis, (b) the binding rate coefficients, k_1 and k_2, for a dual-fractal analysis, and (c) the dissociation rate coefficient, k_d, for a single-fractal analysis are presented in Table 2A. The values of (a) the fractal dimension, D_f, for binding for a single-fractal analysis, (b) the fractal dimensions, D_{f1} and D_{f2}, for binding for a dual-fractal analysis, and (c) the fractal dimension, D_{fd}, for the dissociation phase for a single-fractal analysis are presented in Table 1B. In this case, K_1 is equal to 8.46 and K_2 is equal to 5.15. The affinity value decreases by a factor of 0.61 as one goes from the first to the second phase of binding.

Fig. 3E shows the binding of 20 μl of B cells+VEE virus strain 3880 subtype 1d to pathogen-specific B cells immobilized on a biosensor surface. Once again, a dual-fractal analysis is required to adequately describe the binding kinetics. The dissociation kinetics is adequately described by a single-fractal analysis. The values of (a) the binding rate coefficient, k, for a single-fractal analysis, (b) the binding rate coefficients, k_1 and k_2, for a dual-fractal analysis, and (c) the dissociation rate coefficient, k_d, for a single-fractal analysis are presented in Table 2A. The values of (a) the fractal dimension, D_f, for binding for a single-fractal analysis, (b) the fractal dimensions, D_{f1} and D_{f2}, for binding for a dual-fractal analysis, and (c) the fractal dimension, D_{fd}, for the dissociation phase are presented in Table 2B. In this case, K_1 is equal to 6.27 and K_2 is equal to 48.59. The affinity value increases by a factor of 7.75 as one goes from the first to the second phase of binding.

Fig. 3F shows the binding of 20 μl of B cells+VEE virus strain subtype 1e (Mena II) to pathogen-specific B cells immobilized on a biosensor surface. Once again, a dual-fractal analysis is required to adequately describe the binding kinetics. The dissociation kinetics is adequately described by a single-fractal analysis. The values of (a) the binding rate coefficient, k, for a single-fractal analysis, (b) the binding rate coefficients, k_1 and k_2, for a dual-fractal analysis, and (c) the dissociation rate coefficient, k_d, for a single-fractal analysis are presented in Table 2A. The values of (a) the fractal dimension, D_f, for binding for a single-fractal analysis, (b) the fractal dimensions, D_{f1} and D_{f2}, for binding for a dual-fractal analysis, and (c) the fractal dimension, D_{fd}, for the dissociation phase for a single-fractal analysis are presented in Table 2B. In this case, K_1 is equal to 3.73×10^{-5} and K_2 is equal to 8.6×10^{-8}. The affinity value decreases by a factor of 433.7 as one goes from the first to the second phase of binding.

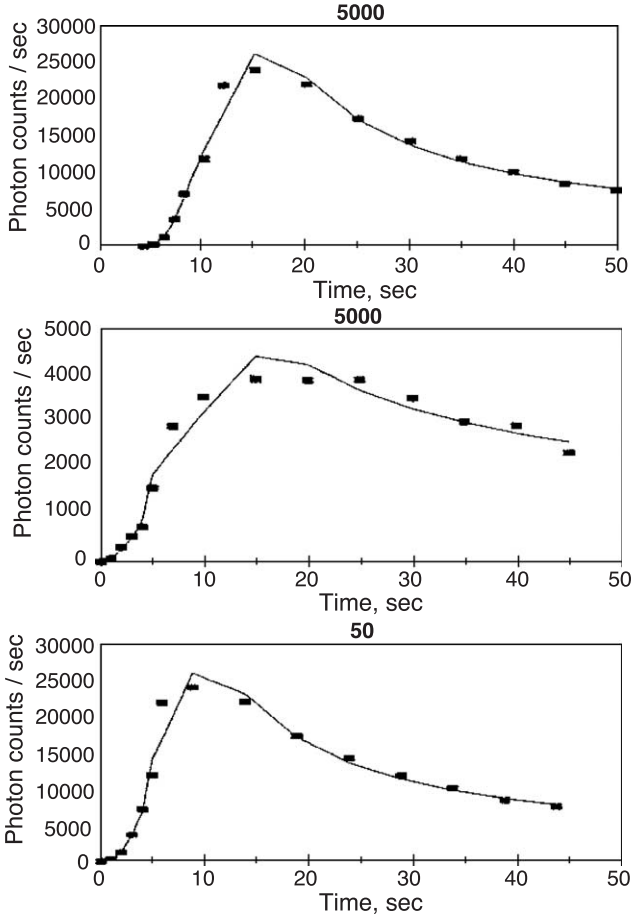

Fig. 4. Binding and dissociation curves for the detection of *E. coli* strain 50 0157:H7 at different concentrations by the B lymphocyte-based biosensor (Rider et al., [10,11] supplement, 2003): (A) 5000 cfu, (B) 500 cfu, and (C) 50 cfu.

Fig. 4A shows the binding of 5000 cfu *E. coli* strain 50 0157:H7 to pathogen-specific B cells immobilized on a biosensor surface. A dual-fractal analysis is required to adequately describe the binding kinetics. The dissociation kinetics is adequately described by a single-fractal analysis. The values of (a) the binding rate coefficient, k, for a single-fractal analysis, (b) the binding rate coefficients, k_1 and k_2, for a dual-fractal analysis, and (c) the dissociation rate coefficient, k_d, for a single-fractal analysis are presented in Table 3A. The values of (a) the fractal dimension, D_f, for binding for a single-fractal analysis, (b) the fractal dimensions, D_{f1} and D_{f2}, for binding for a dual-fractal analysis, and (c) the fractal dimension, D_{fd}, for the dissociation phase are presented in Table 3B. In this case, K_1 is equal to 6.21×10^{-4} and K_2 is equal to 3.59×10^{-3}. There is an increase by a factor of 5.78 in the affinity value as one goes from the first to the second phase of binding.

Due to the 'convex' nature (S-shaped curve) of the binding curve at time, t, close to zero, the fractal dimension value is estimated to be equal to zero (either D_f or D_{f1}). However, D_{f2} (for a dual-fractal analysis) does have a non-zero value. D_{f2} equals 0.7108. Note that it does, however, have a large error estimate, equal to 1.06. Only a positive error (or range) is given, that is D_{f2}=0.7108+1.06, since a negative fractal dimension value has no physical significance. Similarly, the start of the dissociation curve also exhibits an "S-shaped" curvature. Thus, D_{fd} is also estimated to be equal to zero.

Fig. 4B shows the binding of 500 cfu *E. coli* strain 50 0157:H7 to pathogen-specific B cells immobilized on a biosensor surface. A dual-fractal analysis is required to adequately describe the binding kinetics. The dissociation kinetics is adequately described by a single-fractal analysis. The values of (a) the binding rate coefficient, k, for a single-fractal analysis, (b) the binding rate coefficients, k_1 and k_2, for a dual-fractal analysis, and (c) the dissociation rate coefficient, k_d, for a single-fractal analysis are presented in Table 3A. The values of (a) the fractal dimension, D_f, for binding for a single-fractal analysis, (b) the fractal dimensions, D_{f1} and D_{f2}, for binding for a dual-fractal analysis, and (c) the fractal dimension, D_{fd}, for the dissociation phase are presented in Table 1B. In this case, K_1 is equal to 0.00243 and K_2 is equal to 0.0173. There is an increase by a factor of 7.12 in the affinity value as one goes from the first to the second phase of binding.

Once again, due to the 'convex' nature (S-shaped curve) of the binding curve at time, t, close to zero, the fractal dimension curve is estimated to be equal to zero (either D_f or D_{f1}). However, D_{f2} (for a dual-fractal analysis) does have a non-zero value. D_{f2} equals 1.4194±0.5058. Similarly, the start of the dissociation curve also exhibits an "S-shaped" curvature. Thus, D_{fd} is also estimated to be equal to zero.

Table 3B
Fractal dimensions for the binding and the dissociation phase for *E. coli* on a B lymphocytes-based sensor (Rider et al. [10,11], Science Supplement)

Pathogen concentration	D_f	D_{f1}	D_{f2}	D_{fd}
E. coli 5000 cfu strain 50 0157:H7	na	0	0.7108+1.06	0
E. coli 500 cfu strain 50 0157:H7	na	0	1.4194±0.5058	0
E. coli 50 cfu strain 50 0157:H7	0	0	0	0.9310+1.4764

Fig. 4C shows the binding of 50 cfu *E. coli* strain 50 0157:H7 to pathogen-specific B cells immobilized on a biosensor surface. A dual-fractal analysis is required to adequately describe the binding kinetics. The dissociation kinetics is adequately described by a single-fractal analysis. The values of (a) the binding rate coefficient, k, for a single-fractal analysis, (b) the binding rate coefficients, k_1 and k_2, for a dual-fractal analysis, and (c) the dissociation rate coefficient, k_d, for a single-fractal analysis are presented in Table 3A. The values of (a) the fractal dimension, D_f, for binding for a single-fractal analysis, (b) the fractal dimensions, D_{f1} and D_{f2}, for binding for a dual-fractal analysis, and (c) the fractal dimension, D_{fd}, for the dissociation phase for a single-fractal analysis are presented in Table 3B. In this case, K_1 is equal to 122.43 and K_2 is equal to 0.109. There is a decrease by a factor of 1123.21 in the affinity value as one goes from the first to the second phase of binding.

Here also, due to the 'convex' nature (S-shaped curve) of the binding curve at time, t, close to zero, the fractal dimension curve is estimated to be equal to zero (either D_f, D_{f1}, or D_{f2}); D_{fd} has a non-zero value. In this case, since the start of the dissociation curve does not exhibit an "S-shaped" curve, the D_{fd} value is equal to 0.9301+1.4764. There is a large error estimate, thus only the positive error (or range) is presented.

4. Conclusions

A fractal analysis is presented for the binding and dissociation kinetics exhibited by pathogens such as *F. tularensis*, *Y. pestis*, *B. anthracis*, Venezuelan equine encephalitis (VEE) virus, Vaccinia virus, and *E. coli* using

Table 3A
Binding and dissociation rate coefficients for *E. coli* on a B lymphocytes-based sensor (Rider et al. [10,11], Science Supplement)

Pathogen concentration	k	k_1	k_2	k_d
E. coli 5000 cfu strain 50 0157:H7	na	292.2±30.69	1686±429.77	470,246±18,189.7
E. coli 500 cfu strain 50 0157:H7	na	72.39±15.30	515.50±118.40	29,839±2670.9
E. coli 50 cfu strain 50 0157:H7	328.09±101.42	327,417±14,530.1	292.2±30.69	2674.22±986.91

a CANARY (cellular analysis and notification of antigens risks and yields) biosensor [10,11]. The binding and dissociation kinetics may be adequately described by either a single-, dual-, or triple-fractal analysis. A double-fractal analysis was used only if a single-fractal analysis did not provide an adequate fit. This was determined by a regression analysis provided by Sigmaplot (1993).

Due to the dilute nature of the analyte(s) present in the environment, a triple-fractal analysis was used, when necessary, to adequately describe the binding kinetics. This was noted at the lower end of the analyte concentration spectrum analyzed for the VEE virus (5000 pfu, dual-fractal analysis; 500 pfu, triple-fractal analysis), and for *B. anthracis* (10,000 cfu, dual-fractal analysis; 1000 cfu, triple-fractal analysis). Only two data sets are presented here. However, if this trend is observed for the detection of other pathogens, then this makes the detection of these pathogens at their lower end of the concentration spectrum more and more challenging. This is further exacerbated by the fact that the dilute nature of the analyte also leads to variation in the original experimental data of [10,11], although this is not present in this analysis, since only discrete points at regular intervals were taken to model the kinetics.

The change from the binding rate coefficients, k_1 to k_2 to k_3, indicates a change in the binding mechanism on the biosensor surface. Also, this change in the fractal dimension, D_{f1} to D_{f2} to D_{f3}, indicates a change in the degree of heterogeneity on the surface. For example, for the VEE virus at 500 pfu concentration, in about 25 s (duration of the binding phase) there is a double change in the binding mechanism (from k_1 to k_2; and from k_2 to k_3). At 5000 pfu VEE concentration in about 15 s (duration of the binding phase), there is a single change in the binding mechanism (from k_1 to k_2).

In a general sense, fractal models are fascinating. Newer avenues are required to analyze and help detect pathogens at very dilute concentration levels. The analysis of the studies of the boundaries (scale) over which the fractal behavior occurs should prove useful. The real interesting test of the fractal model would be if it can make a prediction that turns out to be correct. This would prove to be extremely valuable, especially in the detection of pathogens. For example, if the fractal analysis enhances (or predicts) a biosensor performance parameter(s), such as stability, sensitivity, response time, etc., as an experimental variable is changed, then the value of the analysis will be substantially increased. Any increase in time that is made available to help in the evacuation process (for example, by making better biosensors) after the establishment of a pathogenic threat is invaluable.

September 11 has emphasized the crucial importance of the timely detection of pathogens. This has been emphasized recently by [15]. These authors used the entropy method of analysis, the Complex Analysis of Sequences via Scaling AND Randomness Assessment (CASSANDRA) algorithm to help enhance the sensitivity of biosensors to a very poisonous substance, tetrodotoxin. It is a worthwhile endeavor to continuously aim to improve the biosensor performance parameters. The immobilization of the receptors on the biosensor surface will lead to some degree of heterogeneity on the biosensor surface. This degree of heterogeneity made quantitative by the fractal dimension very significantly affects the binding and the dissociation rate coefficient. Furthermore, manufacturers like the Biacore (2002) surface plasmon resonance (SPR) claim that diffusional effects are either not present or their effects may be neglected if the biosensor is run properly. This is definitely not the case. A better understanding of the kinetic aspects will significantly help improve the biosensor performance parameters such as stability, sensitivity, selectivity, and response time. This becomes critical in the detection of toxicants [15], and pathogens [16]. What is required is (a) an understanding that both diffusional aspects and heterogeneity are present on the biosensor surface, and (b) one should devise methods by which the effects of these may be separated, and their individual influence on biosensor performance parameters be evaluated. That is the goal of future studies using fractal analysis methods.

Finally, it should be borne in mind that different laboratories use different technologies or slightly different technologies or different experimental designs to analyze and to obtain the rate coefficients and the affinity values for different analyte–receptor reactions. Surely, the comparison of data between different technologies and experimental designs and conclusions thereof should be done with great caution. It is recommended that in vitro methods cannot be viewed as anything else than a diagnostic tool. However, the present analysis is of value in that it provides pros and cons of different in vitro technologies. This makes the user of the technology aware of the quality of the data generated and what can be done to improve the analysis.

References

[1] A. Alwing, Biowarfare defense sensors: applications and research, keynote address, The First IEEE International Conference on Sensors, IEEE Sensors 2002, Orlando, Florida, June 11–14, 2002.

[2] J.P. Fitch, E. Raber, D.E. Imbro, Technology challenges in responding to biological or chemical attacks in the civilian sector, Science 302 (21) (2003 (November)) 1350–1354.

[3] F.S. Ligler, Optical biosensors for the detection of biological warfare agents, Session on Chemical Methods for Biological Detection, Illicit Substance Detection: Chemical/Biological Agents, Mount Holyoke College, South Hadley, MA, June 24–29, 2003.

[4] M. Stowers, On-line bioaerosol characterization using time-of-flight mass spectrometry and laser-induced fluorescence, Session on Physical Methods for Biological Detection, Illicit Substance Detection, Chemical/Biological Agents, D. Franz, T.A. Kovacs, co-chairs, Mount Holyoke College, South Hadley, MA, June 24–29, 2001.

[5] S. Salamone, Bio-IT World, Nanotechnology electrifies biological agent detection, April 18, 2003, http://www.bio-it world. Com/news/041803-report 2370.html.
[6] Defense Advanced Research Projects Agency (DARPA), Special Projects Office, SIMBAD program, 2004, http://www.darpa.mil/spo/programs/simbad.htm.
[7] P. Sveshnikov, Fast and sensitive immunoassays for pathogen detection, Session on Rapid Detection of Infections by Bioterrorism Agents, Illicit Substance Detection, Chemical/Biological Agents, D. Franz, T.A. Kovacs, co-chairs, Mount Holyoke College, South Hadley, MA, June 24–29, 2001.
[8] B. Schneider, Optical Engineering, SPIE, Belligham, Washington, USA, 2002 (April), Special Focus Section.
[9] X. Song, J. Shi, B. Swanson, Flow-cytometry-based biosensor for detection of multi-valent proteins, Anal. Chem. 284 (2000) 35–41.
[10] T.H. Rider, M.S. Petrovic, F.E. Nargi, J.D. Harper, E.D Schwoebel, R.H. Mathews, D.J. Blanchard, L.T. Bortolin, A.M. Young, J. Chen, M.A. Hollis, A cell-based sensor for rapid identification of pathogens, Science 301 (11) (2003 (July)) 213–215.
[11] T.H. Rider, M.S. Petrovic, F.E. Nargi, J.D. Harper, E.D Schwoebel, R.H. Mathews, D.J. Blanchard, L.T. Bortolin, A.M. Young, J. Chen, M.A. Hollis, A cell-based sensor for rapid identification of pathogens, Science 301 (11) (2003 July) 213–215, Online, http://www.sciencemag.org/cgi/content/full/031/5630/213/DC1.
[12] S. Havlin, Molecular diffusion and reactions, in: D. Avnir (Ed.), The Fractal Approach to Heterogeneous Chemistry: Surfaces, Colloids, Polymers, Wiley, New York, 1989, pp. 251–269.
[13] A. Sadana, A fractal analysis for the evaluation of hybridization kinetics in biosensors, J. Colloid Interface Sci. 151 (1) (2001) 166–177.
[14] A. Ramakrishnan, A. Sadana, A single-fractal analysis of cellular analyte–receptor binding kinetics using biosensors, BioSystems 59 (2001) 35–51.
[15] M. Ignaccolo, P. Grigolini, G. Gross, Towards the timely detection of toxicants, Chaos, Solitons Fractals 20 (2004) 87–93.
[16] D.A. Stenger, G.W. Gross, E.W. Keefer, K.M. Shaffer, J.D. Andreadis, W. Ma, Detection of physiologically active compounds using cell-based biosensors, Trends Biotechnol. 19 (2001) 304.
[17] Swanson, B., Session on Rapid Detection of Infections by Bioterorism Agents, Illicit Substance Detection, Chemical/Biological Agents, D. Franz, T.A. Kovacs, co-chairs, Mount Holyoke College, South Hadley, MA, June 24–29, 2001.
[18] A. Sadana, A. Ramakrishnan, A kinetic study of analyte-receptor binding and dissociation to biosensor applications: a fractal analysis for cholera toxin and peptide-protein interactions, Sensors & Actuators B 85 (2002) 61–72.
[19] C.K. Lee, S.L. Lee, Multi-fractal scaling analysis of reactions over fractal surfaces, Surface Science 325 (1995) 294–310.